Radiological injuries under low energy x-rays in mice depending on dose and protocol: comparative characterization of lesion severity and impact of the in vivo bone response on retrospective dose estimations

Manon Guillou, Bruno L'Homme, François Trompier, Anass Errabii, Tifanie Marcoux, Gaëtan Gruel, Yolanda Prezado, Morgane dos Santos

Radiological injuries under low energy x-rays in mice depending on dose and protocol: comparative characterization of lesion severity and impact of the *in vivo* bone response on retrospective dose estimations

Manon Guillou[1], Bruno L'Homme[1], François Trompier[2], Anass Errabii[1], Tifanie Marcoux[1], Gaëtan Gruel[1], Yolanda Prezado[3] and Morgane Dos Santos[1,*].

[1]Institute for Radiological Protection and Nuclear Safety (IRSN), Department of RAdiobiology and regenerative MEDicine (SERAMED), Laboratory of Radiobiology of Accidental exposures (LRAcc) Fontenay-aux-Roses, France;
[2]Institute for Radiological Protection and Nuclear Safety (IRSN), Department of DOSimetry, (SDOS), Ionizing Radiation Dosimetry Laboratory (LDRI), Fontenay-aux-Roses, 92260, France
[3]Institut Curie, University Paris Saclay, PSL Research University, Inserm U 1021-CNRS UMR 3347, Orsay, France.
*Author to whom any correspondence should be adressed

E-mail: morgane.dossantos@irsn.fr
Keywords : dosimetry, EPR spectroscopy, radiological injuries, accidental overexposures, low-energy x-ray

Abstract

Objective:To improve our knowledge about the biological effects of over exposures involving low-energy X-rays, we developed and characterized a preclinical mouse model allowing to mimic different lesion severity degrees induced by 80 kV X-ray depending on the dose and protocol (single or repeated exposure).

Approach: Mice were locally exposed (paw) to 80 kV X-rays in a single (15, 30 or 45 Gy in Kair) or repeated exposition (2x15 or 3x15 Gy in Kair) to assess different degrees of lesion severity. Six post-irradiation euthanasia time points (0, 7, 14, 21, 42, and 84 days) were determined to follow up the evolution of lesions based on the lesion score, weighing and cutaneous blood perfusion. The bone dose was estimated at the different time points by Electron Paramagnetic Resonance (EPR) spectroscopy.

Main results:The monitoring of the lesion severity allows to classify the exposure protocols according to their severity. EPR spectroscopy measurements allow to determine the bone dose on the day of irradiation which is 7 times higher than the initial dose for single protocols. However, the initial signal measured at the end of the repeated exposure was 27% lower than the signal measured for a single dose. The study of the kinetics of EPR signal showed a decrease of the EPR signal which is dependent on the exposure protocol but not on dose highlighting the impact of bone physiology on the bone dose estimation.

Significance: the preclinical model developed allows to assess the impact of the dose and protocol on the lesion severity induced by low-energy X-ray. For the first time, the dynamics of free radicals have been quantified in an *in vivo* model, highlighting that the doses actually administered can be underestimated if samples are taken weeks or even months after exposure.

1. Introduction

The usefulness of ionizing radiation has been well-established since its discovery. However, the harmful effects of these radiations have also been observed since the first applications (Gagliardi and Almond 1996, Berlin 2001). Although the use of ionizing radiation is most often mastered and controlled, it can lead to significant overexposure in accidental or malicious situations. Several publications have listed cases of accidental overexposure (Oliveira 1987, Chambrette et al 2001, Coeytaux et al 2015, Thorne 2022) and online databases also exist, such as the Johnston archives (Johnston Archives 2022), which list the different details of radiation accidents (source, industrial environment, criticality, medical accidents) involving either a single person or a large number of people. A more recent publication by Coeytaux et al (2015) lists and analyzes radiation accidents between 1980 and 2013: 634 accidents were reported and 31% of them involve low-energy x-rays (fluoroscopy).

These accidents, leads mainly to localized overexposure, resulting in the apparition of severe deterministic effects in the days, weeks, or months following the exposure and ranging from erythema to tissue necrosis when a cutaneous dose of 10 Gy is exceeded (International atomic energy agency 1998). One particularity of this low- energy radiation is that its rapid attenuation leads to a very steep dose gradient. Moreover, the heterogeneity of the absorbed dose is reinforced by the predominance of the photoelectric effect at these energies, with an absorbed dose that depends strongly on the atomic number of the materials (Z3 to Z5), leading, for example, to a higher absorbed dose in dense tissues such as bone when compared with soft tissues (Chow and Jiang 2012). As a result, the dose absorbed by deep bone tissue can be much higher than the dose absorbed by the skin. Accurate knowledge of the dose absorbed by the different tissues, including bone, is therefore a major concern in order to help diagnose and treat victims. In addition, our lack of knowledge of the biological consequences of low energy radiation due to the heterogeneous nature of dose deposition makes the prognosis very uncertain for the different tissues, especially for bone. Developing a preclinical experimental model is therefore essential to improve knowledge of the biological effects of this exposure, estimate the dose absorbed by the different tissues, and characterize radiopathological particularities.

To this end, a preclinical model in which the left paws of mice were exposed was developed at the SARRP platform to mimic potential overexposure that can occur with low-energy x-ray radiation (80 kV) (Guillou et al 2022). This previous work, enabled to determine the dose absorbed by the different tissues by Monte Carlo simulations and validated experimentally the bone dose on the day of irradiation by electron paramagnetic resonance (EPR) spectroscopy measurements (Guillou et al 2022). Indeed, EPR spectroscopy has been used for retrospective dosimetry for several years to assess bone doses in the event of radiological accidents (Brady et al 1968, Trompier et al 2009), as bone tissue is one of the most frequently used materials in the field of EPR retrospective dosimetry (journal of the icru 2019). This technique can be used to estimate the dose absorbed by a material by measuring the amount of radicals or defects created in the material in question as a result of exposure to ionizing radiation. The quantity of radicals formed is in proportion to the dose absorbed by the material, and this relationship can be established between the intensity of the EPR signature (in proportion to the number of radicals) and the absorbed dose. This method can thus be used to evaluate the dose absorbed by dental enamel, nails, or the dose detected in bone biopsies, for example. In particular, bone samples have been used in several accident cases to determine an absolute bone dose (Internation Atomic Energy Agency 2004, Clairand et al 2006, Trompier et al 2007). However, in the event of an accident, the biological samples compatible with use in dosimetric measurements, such as bones, are generally taken weeks, months or even years after exposure, and even if radiation-induced free radicals (RIFRs) in bone are known to be stable in extracted bones (Journal of the ICRU 2019), in living bone, a loss of RIFR may be suspected due to the bone physiology. Therefore, this could lead to an underestimation of the initial absorbed dose, and the measured doses may have to be corrected. However, more knowledge is required about the impact of bone physiology on estimated doses, variability, and dependence, as no published data exist (Journal of the ICRU 2019).

Thus, this work aimed to use a preclinical model to characterize radiological burns in the event of accidental overexposure to low energy x-rays (80 kV) depending on the dose and protocol (single or repeated exposure). The potential bias in EPR retrospective dose estimation at different time points

(from 0 to 84 d after irradiation) due to the impact of the biological response of living bone to ionizing radiation was assessed for the first time.

2. Materials and methods

2.1. Irradiation platform and reference dosimetry measurements

Mice paws were locally irradiated with high doses at the Small Animal Radiation Research Platform (SARRP, XSTRAHL Ltd, UK) (Wong et al 2008), in order to mimic accidental overexposure, resulting in radiological burns. The preclinical model used in this work is described in detail in Guillou et al (2022). Briefly, the x-ray source is set to 80 kV and 24 mA, with an inherent filtration of 0.8 mm of beryllium and an additional filtration of 0.15 mm of copper. The homemade brass collimator is used to assess a 4.3 × 4.3 cm2 irradiation field at a distance of 22.5 cm from the x-ray source. The half-value layer is measured experimentally at 0.138 ± 0.006 mm of copper using the protocol described in Dos Santos et al (2021). All reference dosimetry measurements are taken with a flat ionization chamber (PTW TM23342 SN2587), specific to low-energy x-ray radiation, and calibrated in air kerma-free in air (Kair). For this configuration, the mean dose rate is 1.66 ± 0.07 Gy min−1 in Kair with an overall uncertainty of 5% at k = 2.

2.2. Mice and experimental protocol

Adult male C57BL/6JRj mice from Janvier Labs, aged 8 weeks at the beginning of the study, were used. They were housed in an enriched environment (cardboard and cotton dome) in groups of 4 with a 12–12 day-night cycle and unlimited access to food and water in the institute's animal facility, accredited by the French Ministry of Agriculture. The animals were paid close and careful attention as the experimental model can lead to severe radiological burns.

After one week of habituation, the hind paws of the mice were depilated using a clipper and commercial depilatory cream under gas anesthesia (isoflurane 5% for induction, then 2.5%). Three days later, the left hind paw of the mice was irradiated under chemical anesthesia by the intraperitoneal injection of 250 µl of a mixture of 100 mg kg−1 ketamine (Imalgene 1000, Merial, France) and 10 mg kg−1 xylazine (Rompoun 2%, Bayer Healthcare, France). Single expositions of 15, 30, and 45 Gy (Kair) or repeated expositions of 2 × 15 and 3 × 15 Gy (kair) at one week apart were delivered to assess different degrees of lesion severity and mimic potential repeated exposure in patients undergoing interventional radiology. Six post-irradiation euthanasia time points (0, 7, 14, 21, 42, and 84 d) were determined to follow up the evolution of lesions and performed bone dose estimation by EPR spectroscopy. Each group included 8 mice.

2.3. Monitoring variation in the radiation-induced burns over time

The degree of severity of the different protocols was evaluated using the groups kept alive for the longest (D84). Severity was evaluated based on the analysis of the lesion score, the weight of the animals, and the cutaneous blood perfusion.

A lesion scoring system was set up to evaluate the kinetics of radiation-induced lesions macroscopically. The scoring is based on 5 criteria: lesion extent, erythema, edema, paw retraction, and moisture. Erythema, edema, and moisture are assessed in comparison to the non-irradiated lateral control hind paw. The extent of the lesion is assessed based on hair regrowth. The retraction of the hind paw is evaluated in comparison to the non- irradiated lateral hind paw, the displacement of the mice, and the use of its irradiated hind paw. A score between 0 and 1 is assigned for each criterion and for each mouse. A total lesion score is then calculated up to 84 d after irradiation by adding the scores for each criterion together. This assessment was performed in consultation with at least two experimenters every 2 or 3 d throughout the experiment and once a day for the 20 d around the lesion peak.

Then, weight was monitored, and photographs taken every 2–3 d throughout the monitoring period for lesions. In addition to grimace scales (Langford et al 2010), variation in the weight of the animals provides information as a basis for ensuring effective feeding and healthy welfare.

Finally, the moordLDI2 laser Doppler (Moor Instruments, United Kingdom) is a non-invasive, painless imaging technique with non-contact measurements, which can be used to measure cutaneous blood perfusion. These measurements were taken once a week for the group kept 84 d for each irradiation protocol. Due to hair regrowth above the irradiated area or that of the control paw, mice can be shaved again to improve image quality prior to data acquisition. During the acquisition process, the mice were anesthetized under isoflurane (5% for induction, then 2.5%) and positioned on a heating mat set to 37 °C. Measurements are acquired 40 cm from the laser source over a 4.2 cm × 4.2 cm area containing 255 × 255 pixels with a resolution of 165 µm and a 4 ms/ pixel scan speed. In this configuration, the irradiated and non-irradiated (lateral control) hind paw can be acquired on the same image. The image was processed using Python software (Sanner 1999, Milano 2013). Two areas of interest of the same size were defined and used to extract the pixel intensity histograms. An intensity threshold is applied so that the pixels corresponding to the blood flow are retained. A ratio is then calculated between the number of pixels corresponding to the blood flow of the irradiated hind paw and that of the non- irradiated side paw in order to characterize variation in blood flow over time. The Doppler image analysis process is summarized in figure 1.

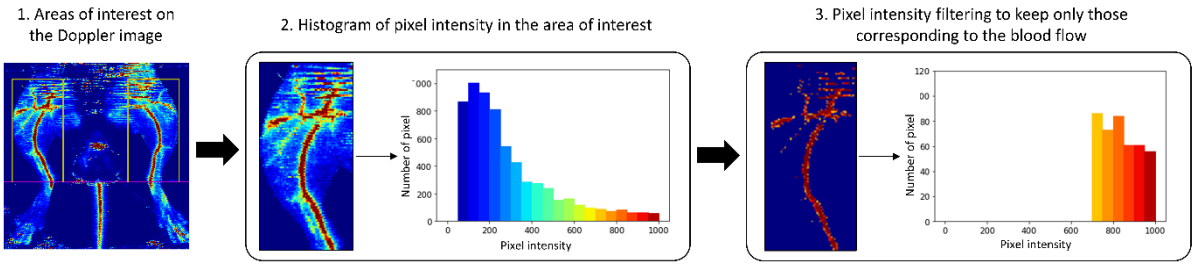

Figure 1: Doppler image analysis used to characterize blood flow over time.

2.4. Experimental bone doses estimated by EPR spectroscopy

EPR spectroscopy is an experimental dosimetry technique used for reference dosimetry measurements with alanine pellets or, in an accidental context, for retrospective dosimetry on biological samples, generally teeth, nails or bones (Trompier et al 2009, Journal of the ICRU 2019). This technique measures paramagnetic species, including those created following exposure to ionizing radiation if sufficiently stable. Thus, this approach can be used to estimate the absorbed dose in a given sample thanks to the proportionality relation between the amount of RIFRs and the absorbed dose.

Sample collection: The irradiated and non-irradiated tibia of mice were collected at 0, 7, 14, 21, 42, and 84 days after irradiation, and used to evaluate: i) the bone dose on the day of irradiation (D0) and ii) variation in the amount of radiation-induced free radicals (RIFR) at different time points (estimated doses). The bones were cleaned, and the bone marrow was flushed with saline solution to remove any traces of soft tissue as far as possible. The tibia samples were then placed in a desiccator for 3 days to be dehydrated, cut into small pieces for EPR measurements, and stored at room temperature.

EPR spectrometer parameters: Measurements were taken with the Bruker EMX in the X-band (9.8 GHz), with an EPR spectrometer supplied with a Q resonator. The spectrometer is located in an air-conditioned room at 20°C (+/-1°C), and operated with the following acquisition parameters: 5 mT for the magnetic field sweep width, 3.99 mW for the microwave power and 0.5 mT for the modulation depth. The EPR spectrum is averaged after acquiring 10 scans. 3 to 5 spectra are acquired per sample while changing the distribution and positions of the bone pieces in order to estimate the reproducibility of measurements.

Estimating the absorbed bone dose: The additive dose method is used to estimate the bone doses and involves re-irradiating the same bone sample with known doses (Desrosiers and Schauer 2001). With this protocol, a calibration curve is for each bone sample using the amplitude measurement range between maximum and minimum (taken at g parallel) for the EPR anisotropic signal of the irradiated bone and the dose added. This individual calibration allows to consider the radiation sensitivity and can be used to evaluate variability between mice in the same group. To construct the calibration curve, 5

additive doses (40, 40, 100, 40 and 40 Gy Kair measured with an ionization chamber calibrated in Kair) were performed with a medical linear accelerator (Synergy®, Elekta) at 10 MV. For the construction of the calibration curves, we have followed the ISO 13304 recommendations, mentioning that, for these energy levels (MV) and for the volume of bone considered, the difference between the dose absorbed by the bone and air kerma measured is very small (International Standard 2020). Dosimetry measurements were taken as follows: dose rate of around 3 Gy min−1 measured with a cylindrical ionization chamber (PTW 31010–0.125CC), a 30 cm × 30 cm irradiation field, a source-sample distance of 1 m, at 180° to the irradiator arm and a 1.5 cm plexiglass plate is added between the samples and the treatment table to achieve the charge equilibrium.

3. Results

3.1. Characterization of radiation-induced burns (score, weight, doppler)

Figure 2 shows representative photographs of the radiobiological burns (Figure 2A) and the evolution of the mean total lesion score with the standard error of the mean (Figure 2B), with a table providing information on various lesion kinetics parameters such as the intensity of the lesion peak, skin damage development kinetics, skin damage healing kinetics and the Area Under the Curve (AUC) of the lesion score .

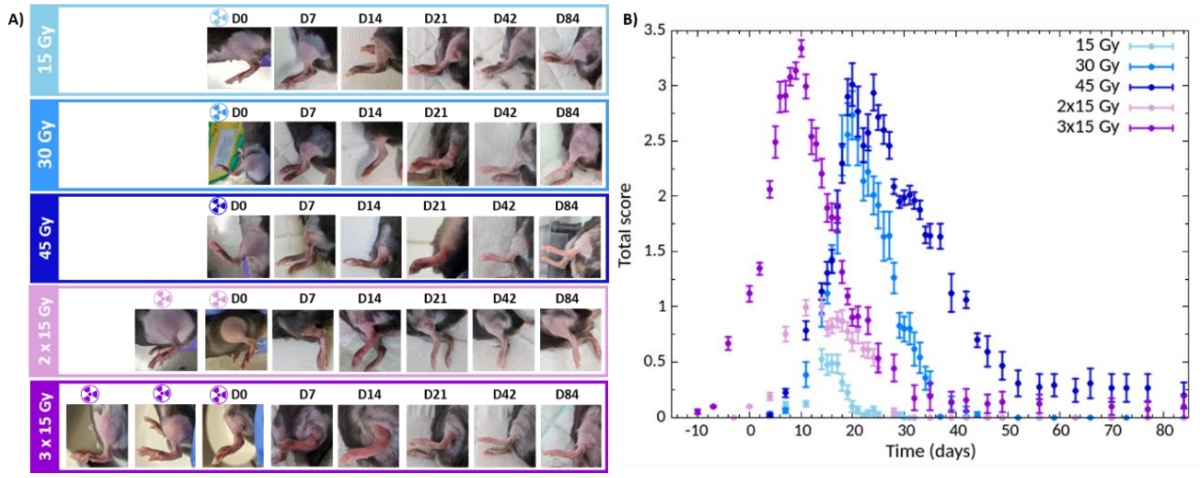

Figure 2: Evaluation of the radiological burns as a function of the dose and protocol. A) Representative photographs of the radiological burn at specific time points and B) evolution of the mean total lesion score with the standard error of the mean over time.

Figure 2 shows that the first signs of skin damage appear one week after irradiation for the single exposure protocol. The peak lesion is reached around 21 days after irradiation for the 30 and 45 Gy group and 17 days after irradiation for the 15 Gy group which developed a minor lesion earlier. Then, the lesions healed, and we observed an apparent total recovery for the 15 and 30 Gy groups and partial recovery for the 45 Gy group. With the repeated exposure protocols, the first signs of skin damage also appeared 7 d after the first irradiation. Consequently, the second and third irradiation were performed in an existing radiation-induced lesion. As for the 30 and 45 Gy groups, the lesion peak is reached around 21 d after initial exposure. An apparent total and partial recovery was observed for the 2 × 15 Gy and 3 × 15 Gy groups respectively. If we compare the protocols leading to the same total dose, the 2 × 15 Gy protocol is less severe than the 30 Gy protocol with a maximum lesion intensity divided by more than two. However, this strong difference was not detected between the 3 × 15 and 45 Gy protocols.

In addition to the total lesion score, Table 1 provides information on different parameters relating to lesion kinetics such as the intensity of the lesion peak, skin damage development kinetics, skin damage healing kinetics and the Area Under the Curve (AUC) of the lesion score.

Table 1: Main parameters used to characterize lesion kinetics

Group	15 Gy	30 Gy	45 Gy	2x15 Gy	3x15 Gy
Maximum score	0.6 ± 0.3	2.9 ± 0.8	3.2 ± 0.5	1.1 ± 0.2	3.4 ± 0.2
Rate of onset of skin damage (slope)	0.05 ± 0.03	0.18 ± 0.05	0.18 ± 0.05	0.07 ± 0.01	0.18 ± 0.02
Healing rate (slope)	0.14 ± 0.05	0.19 ± 0.09	0.10 ± 0.02	0.09 ± 0.03	0.15 ± 0.05
AUC	4.3 ± 1.8	36 ± 8	75 ± 19	17 ± 3	61.± 17

These data highlight that the 30, 45 and 3 × 15 Gy groups are very similar regarding the onset of skin damage (0.18 for each protocol), and maximum lesion score (around 3) but differ in terms of healing rate. As expected, the AUC calculations for the lesion score showed that the more severe the lesions, the higher the AUC.

If we compare the protocol leading to the same total dose, the 2 × 15 Gy protocol is much less severe than the 30 Gy protocols, as all parameters are divided by at least two. Concerning the 3 × 15 Gy and the 45 Gy protocols, the main difference is lesion healing, which is faster for the 3 × 15 Gy protocol, leading to a lower AUC. The relationship between AUC and the retrospective bone dose estimate 84 d after irradiation will be shown in the next section.

To improve our understanding of the kinetics of radiological burns depending on the dose and protocol, Figure 3 shows a detailed analysis of the lesion score with the respective proportions of each criterion as part of the total score (erythema, edema, retraction, extent of the lesion and moisture).

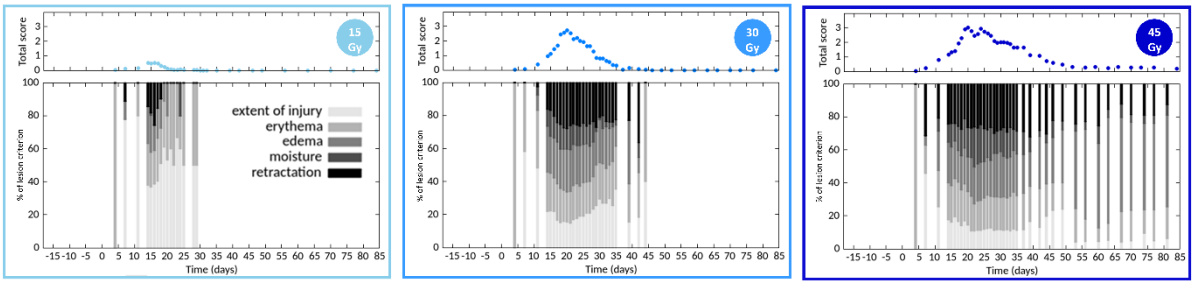

Predominant parameters at the lesional peak

	15 Gy	30 Gy	45 Gy	2x15 Gy	3x15 Gy
Extent of injury	X	X	X	X	X
Erythema	X	X	X	X	X
Edema		X	X	X	X
Moisture		~	X		X
Retraction		X	X	X	X

Figure 3: Analysis of the score as a function of the parameters characterizing the lesion (extent of injury, edema, retractation, erythema and moisture) and the table with information about the predominant parameter at the lesion peak.

These results highlight that, for the 15 Gy group, the lesions are dominated by the extent of the injury and the erythema. For the 2 × 15 Gy protocol, edemas and the paw retraction were also recorded and equally distributed in addition to the extent of the lesion and the erythema. With the 30 Gy group,

moisture appears but less extensively than with the other parameters. The five parameters are equally distributed for the 45 and 3 × 15 Gy groups. For these last two protocols, leading to partial healing, at 84 days post irradiation, the edemas persist for the 45 Gy protocol, especially in the toes, unlike the 3 × 15 Gy protocol where the erythema and extent of the lesion persist.

In addition, cutaneous blood perfusion was also quantified using Doppler images taken each week until 84 d post-exposure. Figure 4 shows representative Doppler images for each exposure protocol and the evolution of the cutaneous blood perfusion over time for each group where the total score was reported as visual guidance and to help identify the lesion peak more easily.

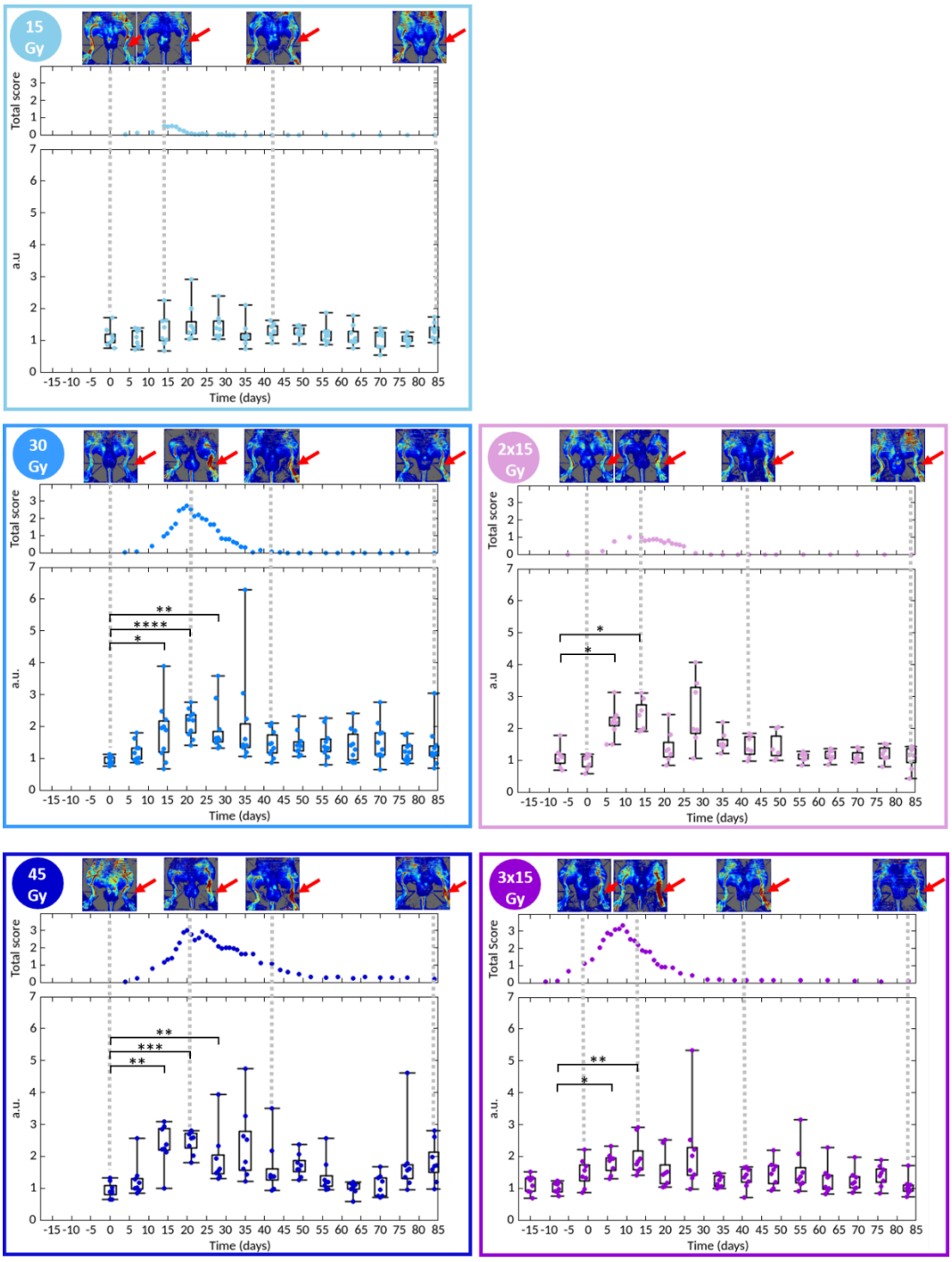

Figure 4: Variation in cutaneous blood perfusion normalized based on the non-irradiated paw over time for each group with representative doppler images. Red arrows indicate the irradiated paw and each dot represent one mouse. Statistical analysis was performed with the kruskall Wallis nonparametric test.

These measurements show a significant increase in cutaneous blood flow perfusion between 14 and 28 d for the 30 and 45 Gy single exposure protocol compared to the initial level of cutaneous blood flow. Cutaneous blood perfusion then tends to its initial level over time. No significant variation in the cutaneous blood perfusion was observed for the 15 Gy group, which developed the most minor lesions. For the repeated exposure protocols, a significant increase in cutaneous blood perfusion was also observed at the lesion peak, i.e. 14 and 21 d after initial exposure for the 2 × 15 Gy group and 21 and 28 d after initial exposure for the 3 × 15 Gy group, but this increase is much less pronounced than for single exposure groups.

Finally, as part of the evaluation of the impact of irradiation on animal welfare, figure 5 shows the mean weight gain with the standard error of the mean for single (figure 5(A)) and repeated (figure 5(B)) exposure protocols compared to their controls.

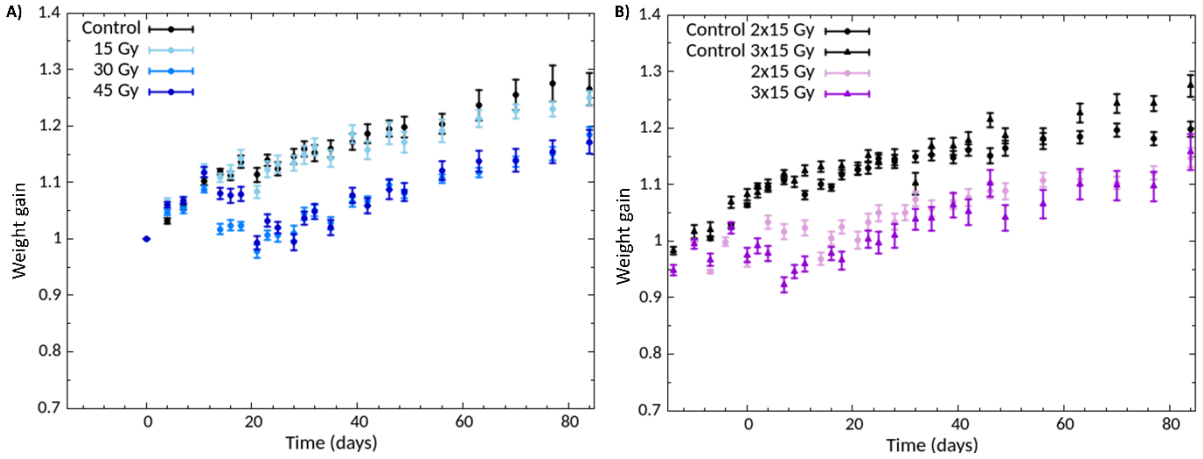

Figure 5: Variation in mean weight gain with the standard error of the mean over time for the single (A) and repeated (B) exposure protocols compared to their controls.

For the single exposure protocols (Figure 5A), no weight loss was observed for the 15 Gy group, and weight gain was similar to the control group. For the 30 and 45 Gy groups, weight loss was observed from day 11 post-exposure, reaching a maximum weight loss at the lesion peak (day 21, 16% compared to their initial weights) and weight was regained from day 25 post-exposure. Similarly, weight loss was also observed for the mice exposed under 2x15 Gy or 3x15 Gy. This weight loss is also maximal at the lesion peak (16% compared to their initial weights) and, once the lesion peak passed, the mice regained weight. In addition, we also observed slight weight loss following each exposure session due to the anesthesia of the mice. Although our irradiation protocols induced severe radiological burns, all mice regained weight after the lesion peak, independently of the initial dose or protocol.

3.2. EPR Dosimetric characterization: estimated absorbed doses for bones and signal loss at different time points

Figure 6 and Table 2 report the bone dose estimated using EPR spectroscopy for mouse tibia at 6 different time points for each irradiation protocol studied.

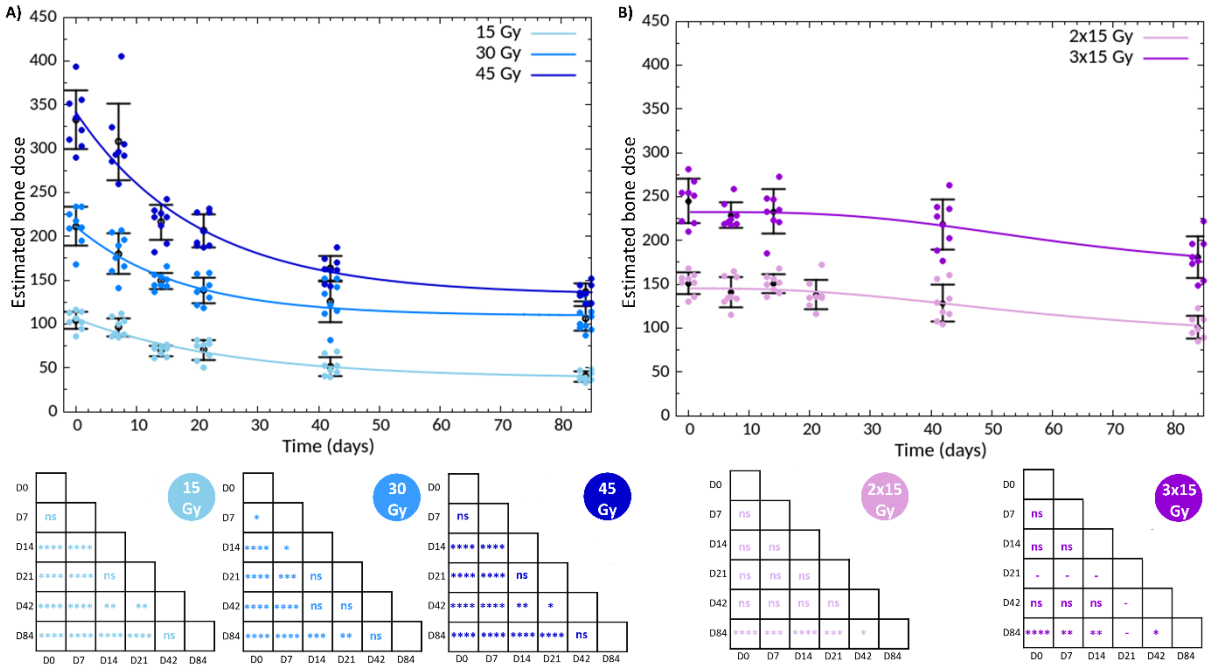

Figure 6: Estimated bone dose (D0) according to EPR spectroscopy for cortical mouse bone samples and characterization of signal loss for 6 different post-irradiation time points for single (A) and repeated (B) exposure protocols. Each dot represents one mouse (lines are plotted as visual guidance). Statistical analysis used to evaluate the decrease in radiation-induced free radicals at different post-irradiation time points for each group is also shown for each protocol (Shapiro test then One-way Anova).

Table 2: Experimentally estimated mean bone dose (D0) according to EPR spectroscopy for cortical bone samples and characterization of signal loss for 6 post-irradiation times (D7, D14, D21, D42 and D84).

Group	***D0***	**D7**	**D14**	**D21**	**D42**	**D84**
15Gy	*104 ± 10 Gy*	96 ± 11 Gy	69 ± 6 Gy	71 ± 12 Gy	52 ± 11 Gy	40 ± 6 Gy
2x15Gy	*151 ± 13 Gy*	141 ± 17 Gy	150 ± 10 Gy	138 ± 17 Gy	128 ± 21 Gy	103 ± 13 Gy
30Gy	*211 ± 22 Gy*	180 ± 23 Gy	150 ± 9 Gy	138 ± 15 Gy	126 ± 24 Gy	106 ± 14 Gy
3x15Gy	*245 ± 25 Gy*	229 ± 15 Gy	233 ± 25 Gy	292 ± 12 Gy	219 ± 29 Gy	181 ± 24 Gy
45Gy	*332 ± 33 Gy*	308 ± 43 Gy	216 ± 20 Gy	206 ± 19 Gy	163 ± 15 Gy	136 ± 10 Gy

For the single exposure protocols, on the day of irradiation (D0), the mean absorbed bone dose was 104 ± 10 Gy, 211 ± 22 Gy, and 332 ± 33 Gy for irradiation of 15, 30, and 45 Gy in Kair respectively. An air-to-bone conversion factor of 7.1 ± 0.7 was determined from these data and the initial irradiation dose at D0 in agreement with the publication of Guillou et al (2022). The signal estimated by EPR spectroscopy, i.e. the quantity of RIFRs, then decreases exponentially with time. In three weeks, the EPR signal is reduced by 32% and tends to stabilize for the later time points. Indeed, 84 d after irradiation, the bone EPR signal decreased by 50%–60%, and accordingly, the corresponding estimated bone dose with bias was only 40 ± 6 Gy, 106 ± 14 Gy, and 136 ± 10 Gy for irradiation of 15, 30, and 45 Gy Kair respectively. According to statistical analysis at different time points for each single exposure group, regardless of the initial dose, no statistical difference was observed between 0 and 7 d, and 14 and 21 d, which may suggest that at least 7 d are needed to detect statistically significant variation in the bone dose measured by EPR spectroscopy. For the later time points, between 42 and 84 d, no statistical differences were observed confirming the tendency for the EPR signal to stabilize 6 weeks post-irradiation.

For the repeated exposure protocols of 2 × 15 or 3 × 15 Gy at one week intervals, the bone dose measured by EPR spectroscopy at D0 is estimated to be 151 ± 13 Gy and 245 ± 25 Gy respectively. Interestingly, these estimated bone doses were more than 25% lower than those measured after a single exposure session at 30 and 45 Gy Kair. Unlike single exposure protocols, a progressive decrease in the estimated EPR dose was observed in the case of repeated exposure. Between the date of irradiation and 84 days after the last exposure, the EPR doses estimated at the bone decreased from 151 ± 13 to 103 ± 13 Gy for the 2 × 15 Gy protocol and 245 ± 25 Gy to 181 ± 24 Gy for the 3 × 15 Gy protocol. Additionally, in the case of repeated exposure, no statistical differences were observed for the measurements taken during the first 42 days following the last irradiation (figure 6(B)).

Moreover, intergroup variability of between 6 and 13% was observed for all doses, protocols and time points.

To compare the temporal dynamic of the EPR signal on the bone dose estimation in the function of the dose and protocol, Figure 7 shows data normalized according to the initial measured mean bone dose at D0 and can be used to compare the dynamics of the EPR signal over time for the estimated bone doses as a function of dose and protocol.

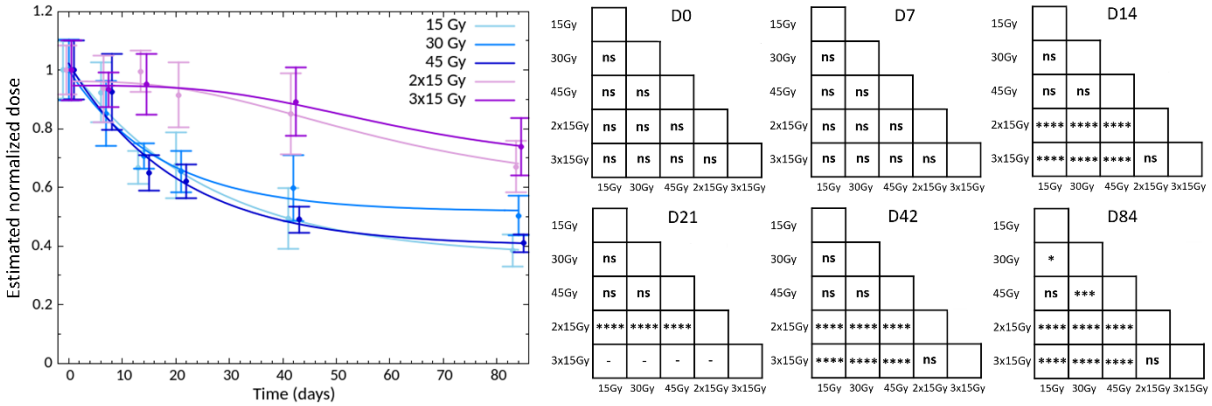

Figure 7: Comparison of the kinetics of the radiation-induced free radicals. A) Mean bone dose with standard error at different post-irradiation time points normalized based on the estimated mean bone dose on the date of irradiation (D0) and B) statistical analysis comparing the groups at the 6 specific time points (Shapiro test then One-way Anova).

These results further highlight the two types of RIFR kinetics, which depend on the type of exposure (single or repeated) but not on the dose administered. As mentioned above, the EPR signal decreased rapidly (32%) over the first three weeks and then continued to decrease, tending to stabilize in the longer term, with a loss of about 36% between D21 and D84, i.e. a mean underestimation of the dose measured for the bone of 59% 3 months after irradiation. Regarding repeated exposure protocols, the kinetics are identical but very different from those of single exposures. Indeed, the dose measured for bone is stable until 21 d after the last irradiation session with a mean loss of less than 4% but decreases in the long term with an underestimation of 29% 84 d after the last exposure.

We can use statistical analysis at each time point (figure 7) to demonstrate a significant statistical difference between single and repeated exposure from 14 d after exposure.

3.3. Correlation between lesion severity and residual bone dose measured 84 d after irradiation

As part of the exploration of the clinical relevance of the EPR-estimated bone dose measured 84 d after irradiation, figure 8(A) reports the correlation analysis between the bone dose estimated by EPR

spectroscopy 84 d after irradiation and the AUC of the lesion score reported in table 1. Each dot corresponds to a mouse with its bone dose on D84 on the x-axis and its AUC value on the y-axis.

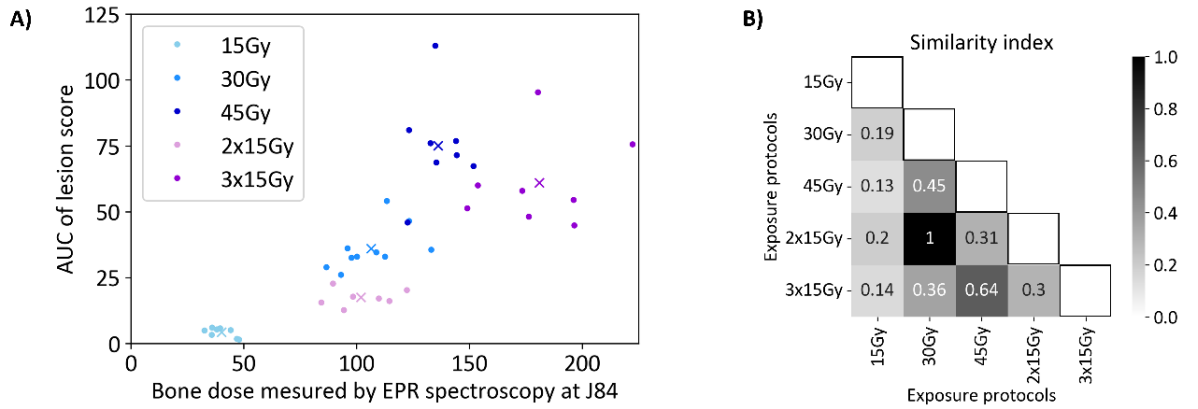

Figure 8: A) Correlation analysis between the dose measured by EPR spectroscopy on D84 and the AUC of the total lesion score, B) Heatmap characterizing similarity between clusters.

These results show that the animals are distributed in distinct clusters (figure 8(A)) and show a correlation between the severity of the lesion and the measured bone dose at D84 by group. However, these results also highlight that the higher AUC does not necessarily correlate with the highest residual EPR signal measured 84 d after irradiation. The similarity index was calculated to analyze the clusters formed, taking into account the dispersion and the Euclidean distance between the barycenter of each cluster. The similarity index between 2 clusters is calculated as the ratio between the total mean distance to the barycenter in each cluster and the distance between the 2 barycenters (Davies and Bouldin 1979). The closer the score is to 1, the closer the clusters are to each other. The data shown in figure 7(B) are normalized based on the maximum similarity value. Thus, the 30 Gy and 2 × 15 Gy clusters are very similar with a normalized similarity index of 1. Similarly, the 45 Gy and 3 × 15 Gy clusters are similar with a similarity index of 0.64. On the contrary, the 15 Gy cluster is very different from all the others with similarity indices not exceeding 0.2. Although the exposure protocols differ, the groups with the same total dose form similar clusters.

4. Discussion

Although fortunately rare, radiological accidents can occur and have severe consequences depending on the dose, the type of exposure, and even the location of the exposure. Victim management can be very complex, especially if low-energy x-ray radiation is involved (<150 kV). Indeed, due to the predominance of the photoelectric effects in this x-ray range, dose deposition is very heterogeneous and depends strongly on the composition and density of the tissue passed through. Preclinical models are therefore an undeniable asset in improving our understanding of the particularities and consequences of this type of exposure. The earlier study by Guillou et al (2022) characterized dose deposition in the different tissues using Monte Carlo simulations as well as experimentally for bone thanks to EPR spectroscopy measurements taken on the day of exposure. This work aimed to complete this earlier study by evaluating the radiobiological burns induced by 80 kV x-ray at different post-irradiation time points as a function of the dose and protocol and by studying the stability of the bone EPR signal in an in vivo preclinical model. Indeed, in the event of a radiological accident, EPR spectroscopy is often used to evaluate an individual dose from biological samples such as dental enamel or nail or via bone biopsies (Trompier et al 2009). However, even if the trapped RIFRs are stable in extracted bone (ex vivo), this is not the case in living bone (in vivo) (Journal of the ICRU 2019). Thus, if the dosimetric measurements are taken several weeks or months after exposure, we can expect the dose to be underestimated depending on many parameters such as the type of exposure, biological material, and age, for example. This study evaluated the dynamics of RIFRs in living bone as part of a

preclinical model and characterized the impact of the dose and protocol at different time points for the first time.

Degrees of lesion severity:

Although mice models for radiation-induced skin syndrome have already been studied in the literature, mainly for high-energy x-ray or gamma radiation (Kumar et al 2008, da Silva Santin et al 2020, Loinard et al 2023), we needed to precisely characterize lesion kinetics as we used low-energy x-ray for which dose deposition is highly dependent on the tissue passed through (Guillou et al 2022). We developed a specific grid score adapted from the METREPOL (Medical TREatment ProtocOLs) system for radiation accident victims (Fliedner et al 2008) to characterize degree of lesion severity over time. The scoring method involved the clinical assessment of 5 parameters, allowing for the more accurate evaluation of skin lesions, unlike the total lesion score generally reported in publications (Kumar et al 2008, Cunningham et al 2021, Loinard et al 2023). Our results showed that, at any dose and protocol, the kinetics of radiological burns are similar in terms of the onset kinetics of the cutaneous symptoms, but the severity and kinetics of healing are very different and depend on the dose and exposure protocol (figure 2 and table 1). The different parameters studied were used to classify the exposure protocols according to their severity: 15 Gy < 2 × 15 Gy < 30 Gy < 3 × 15 Gy < 45 Gy. Our preclinical model showed that different degrees of severity can be achieved: minor with a single exposure session to 15 Gy, moderate with the 2x15 Gy protocol and severe to very severe with the 30, 45, and 3 × 15 Gy protocols, which all differ in terms of the healing process from radiological burns. Despite the same total dose, our results also showed a significant difference in lesion severity between the 2 × 15 Gy and 30 Gy groups, which is consistent with the principle of dose fractionation to minimize side effects on healthy tissue. Interestingly, this effect is not so obvious when comparing the 3 × 15 Gy and 45 Gy conditions. Indeed, the only difference between these last two protocols is healing, which is a little bit faster for the 3 × 15 Gy protocol. Thus, the number of exposure sessions seems to have an impact on lesion severity and healing but the time between exposure sessions must also be taken into account. Indeed, in this work, exposure was repeated at one-week intervals; consequently, the second and the third irradiation sessions were applied to already damaged areas, slight erythema, and radiological burns respectively. These two protocols were initially developed to mimic potential re-exposure in interventional radiology, but exposure session intervals differ from the most representative interventional radiology practices for clinical use. In further work, it would be worth exploring the impact of exposure time intervals and the effect of the dose per session.

However, it was difficult to compare our results with those published in the literature as the preclinical model, irradiation conditions, dose or radiation quality are completely different (Rottensteiner-Brandl et al 2017, Zhai et al 2019, Jullien et al 2023, Loinard et al 2023). Moreover, comparing with data from the literature is also sometimes difficult due to the inadequate information provided on irradiation conditions and dosimetry (Draeger et al 2020, Trompier et al 2023).

Dosimetric characterization:

On the date of irradiation for the single exposure protocol, the bone dose measured experimentally by EPR spectroscopy was 7 times higher than that measured with an ionizing chamber calibrated in Kair. Our results also show that this factor is identical whatever the initial single doses administered. These results agree with our previous publication, where factors of 6.5 ± 0.9 and 6.2 ± 1.0 were found for experimental and simulated data respectively (Guillou et al 2022). With these new results, we can consider improving our numerical model to produce output which is closer to the experimental measured bone dose by taking into account the real bone composition and density. Indeed, our numerical model used predefined material extracted from a code database. On this basis, we can consider using the chemical analysis of bone samples, such as Inductively Coupled Plasma Mass Spectrometry (ICP-MS), to measure elements in bones and integrate these data in our numerical model.

Concerning bone dose estimation at different post-irradiation time points, an increasing underestimation of the bone doses measured by EPR spectroscopy was shown. For single exposure protocols, an

exponential decrease (40% in 3 weeks) in the estimated dose was quantified, which is independent of the initial dose. In addition, for the short irradiation time points, a minimum of 14 d is required to see a statistically-significant difference between groups, which may relate to the period required for complete physiological bone renewal (2 weeks for mice (Jilka 2013)). This indicates that most of the bone-trapped RIFR signal decreased over the first three weeks after exposure. This decrease may indicate repair processes in response to irradiation. It is also important to take note that we still measured an EPR signal three months after exposure, which seemed to stabilize and highlighted that RIRFs remained trapped in the bone matrix. This observation could also suggest that some parts of the bone matrix remained unaffected by the renewal bone processes.

Interestingly, a very different decreasing trend was highlighted for RIFRs for repeated exposure. The initial signal measured at the end of the repeated was 26 to 28% lower than the signal measured for a single dose (i.e. 30 or 45 Gy group). These results show that, unlike ex vivo exposure for which the EPR signals are cumulative, in an in vivo preclinical model, the doses are not cumulative for each fraction. Several hypotheses could be considered regarding this reduction on the day of the last irradiation session. Firstly, we could hypothesize that a biological response occurs between the first two irradiation sessions releasing the RIFRs trapped in the crystals. Then, during the second irradiation session, new RIFRs would be created and trapped in the calcium hydroxyapatite crystals. Another potential hypothesis explaining the reduction in EPR signal is that the bone structure is modified and cannot trap the RIFRS in the same way. This lower initial signal (i.e. estimated dose) thus seems to behave in a similar manner to the signal observed for single doses from the third week after exposure with a low rate of decrease.

These results probably highlight the impact of bone turnover on the bone dose estimate. Indeed, it is well known that bone tissues are constantly metabolically active and undergo continuous remodeling and regeneration even once the bone has reached maturity (Siddiqui and Partridge 2016). This bone remodeling is required to repair bone damage, including radiation-induced damage. Thus, even if the CO2- free radicals trapped in the hydroxyapatite matrix are long-lived, the biological processes set in motion following irradiation to repair the radiation-induced damage will impact the quantity of free radicals measured and therefore the dose. Very few data are available in the literature on the impact of bone turnover on bone dose estimates a long time after exposure. We could cite the study by Kreft et al (2014), in which bone biopsies were performed on patients having received radiotherapy and showed that, for the patient whose biopsy was performed the longest after exposure (6 years), the dose was underestimated. Although bone is mainly targeted for retrospective dosimetry in radiological accidents, our knowledge of the impact of bone physiology and remodeling is inadequate (Journal of the ICRU 2019). Thus, even though our results were obtained in mice, for which bone renewal rates ((0.1% versus 0.7% per day) and the period required for complete remodeling 2 weeks versus 6–9 months) differ to humans (Jilka 2013), this study allowed us to assess the dynamics of RIFRs by studying the effects of doses and protocols for the first time. Micro CT image analysis (bone mineral density, volumes) and histological measurements (histomorphometry) are currently under way aiming to improve our understanding of the biological processes involved in responses to irradiation and tissue damage. These processes aim to correlate the results of these radiopathological studies and our EPR spectroscopy data.

Correlation analysis:

Finally, the correlation analysis between bone doses measured 84 days after irradiation and the AUC was analyzed. According to the calculation of the cluster similarity index, the 30 Gy and 2 × 15 Gy exposure clusters are the most similar, with the 45 Gy and 3 × 15 Gy exposure clusters also being fairly similar. Moreover, although all of the mice in the same group were similarly exposed, the kinetics and healing of the radiation- induced lesions, and doses estimated by EPR spectroscopy varied widely. The average variability of the AUC of the lesion score ranges between 19% and 42%, highlighting the variability of responses between mice. In addition, the bone dose estimated on D84 by EPR spectroscopy varies between 8 and 13%. This variation can mainly be explained by bone composition and density, even for mice of the same age, sex, and strain (Akther et al 2000, Somerville et al 2004, Mumtaz et al 2020). This correlation analysis also showed that the highest AUC did not lead to the

highest dose, and vice versa. These results show the importance of an individual assessment of lesion severity and dose for our model.

5. Conclusions

This study characterized radiation-induced lesions caused by low-energy x-ray (80 kV) and assessed the impact of dose and exposure protocol on the severity of these lesions. In the context of over-irradiation accidents and retrospective dosimetry where bones are commonly used for retrospective dosimetry, the lack of knowledge of the impact of the bone physiology is a major challenge (Journal of the ICRU 2019). This study quantified the dynamics of free radicals at different time points in an in vivo model for the first time, highlighting that the doses actually administered can be underestimated if samples are taken weeks or even months after exposure.

Acknowledgments
The authors would like to thank the GSEA of IRSN for technical assistance especially Romain Granger, Sébastien Mazaudier, Amandine Sache and Delphine Denais-Lalième. We also want to thank Yoann Ristic and Miray Razanajatovo for the irradiation on the medical accelerator.

Data availability statement
All data that support the findings of this study are included within the article (and any supplementary information files).

Declaration of interest
The authors report no conflict of interest. The authors alone are responsible for the content and writing of the paper.

Ethical statement

All the experiments were supervised according to current French (decree 2013-118) and European (EC directives 2010/63/EU) regulations on the use of animals for scientific research projects. Animal use and experimental protocols have been justified and approved by the IRSN ethical committee n°81 (approval number E92-032-01) and authorized by the French Ministry of Research (APAFIS#16160-2018071810588014 v2 and APAFIS#30761-2021033014392127 v2).

References

Akther M P, Iwaniec U T, Covey M A, Cullen D M, Kimmel D B and Recker R R 2000 Genetic variations in bone density, histomorphometry, and strength in mice Calcified Tissue Int. 67 337–44

Berlin L 2001 Radiation-induced skin injuries and fluoroscopy Am. J. Roentgenol. 177 21–5

Brady J M, Aarestad N O and Swartz H M 1968 In vivo dosimetry by electron spin resonance spectroscopy Health Phys. 15 43–7

Chambrette V, Hardy S and Nénot J-C 2001 Les accidents d'irradiation. Mise en place d'une base de données ' ACCIRAD ' à l'IPSN. Radioprotection 1 36 477–510

Chow J C L and Jiang R 2012 Bone and mucosal dosimetry in skin radiation therapy: a monte carlo study using kilovoltage photon and megavoltage electron beams Phys. Med. Biol. 57 3885–99

Clairand I, Trompier F, Bottollier-Depois J-F and Gourmelon P 2006 Ex vivo ESR measurements associated with Monte Carlo calculations for accident dosimetry: application to the 2001 Georgian accident Radiat. Prot. Dosim. 119 500–5

Coeytaux K, Bey E, Christensen D, Glassman E S, Murdock B and Doucet C 2015 Reported radiation overexposure accidents worldwide, 1980–2013: a systematic review PLoS ONE 10 e0118709

Cunningham S et al 2021 FLASH proton pencil beam scanning irradiation minimizes radiation-induced leg contracture and skin toxicity in mice Cancers 13 1012

Davies D L and Bouldin D W 1979 A cluster separation measure IEEETrans Pattern Anal Mach Intell. 1 224–7

Desrosiers M and Schauer D A 2001 Electron paramagnetic resonance (EPR) biodosimetry Nucl. Instrum. Methods Phys. Res.B 184 219–28

Draeger E et al 2020 A dose of reality: how 20 years of incomplete physics and dosimetry reporting in radiobiology studies may have contributed to the reproducibility crisis Int. J. Radiat. Oncol.*Biol.*Phys. 106 243–52

Dos Santos M, Paget V, Trompier F, Gruel G and Milliat F 2021 Dosimetry for cell irradiation using orthovoltage (40–300 kV) x-ray facilities. JoVE 168 e61645

da Silva Santin M et al 2020 Initial damage produced by a single 15 Gy x-ray irradiation to the rat calvaria skin Eur. Radiol. Exp. 4 32

Fliedner T M, Powles R, Sirohi B and Niederwieser D 2008 Radiologic and nuclear events: the METREPOL severity of effect grading system Blood 111 5757–8

Gagliardi R A, Almond P R and Knight N 1996 A history of the radiological sciences Radiol. Centennial 3

Guillou M, L'Homme B, Trompier F, Gruel G, Prezado Y and Dos Santos M 2022 Preclinical modeling of low energy x-rays radiological burn: dosimetry study by monte carlo simulations and EPR spectroscopy Front. Physiol. 13 1075665

International Atomic Energy Agency 2004 Accidental Overexposure Of Radiotherapy Patients in Bialystok

International Atomic Energy Agency 1998 Diagnostic and Treatment of Radiation Injuries (International Atomic Energy Agency)

International Standard 2020 Radiological protection—minimum criteria for electron paramagnetic resonance (EPR) spectroscopy for retrospective dosimetry of ionizing radiation: II. Ex vivo human tooth enamel dosimetry ISO 13304-2:2020(E) Switzerland: International Standard

Jilka R L 2013 The relevance of mouse models for investigating age-related bone loss in humans J. Gerontol.A 68 1209–17

Johnston Archives 2022 Database of radiological incidents and related events disponible sur: database of radiological incidents and related events (Johnstonsarchive.Net) https://johnstonsarchive.net/nuclear/radevents/index.html

Journal of the ICRU 2019 Electron paramagnetic resonance dosimetry J. ICRU 19 46–68

Jullien N, Graziosi E R, Gauthier M, Drouet M, Francois S and Riccobono D 2023 A New murine highly localized high-dose muscle radiation model as a tool to develop innovative countermeasures to treat radio-induced muscular lesions The 2nd Int. Electronic Conf. on Biomedicines MDPI p 49 Disponible sur: https://mdpi.com/2673-9992/21/1/49

Krefft K et al 2014 Application of EPR dosimetry in bone for ex vivo measurements of doses in radiotherapy patients Radiat. Prot. Dosim. 162 38–42

Kumar S, Kolozsvary A, Kohl R, Lu M, Brown S and Kim J H 2008 Radiation-induced skin injury in the animal model of scleroderma: implications for post-radiotherapy fibrosis Radiat. Oncol. 3 40

Langford D J et al 2010 Coding of facial expressions of pain in the laboratory mouse Nat. Methods 7 447–9

Loinard C, Benadjaoud M A, Lhomme B, Flamant S, Baijer J and Tamarat R 2023 Inflammatory cells dynamics control neovascularization and tissue healing after localized radiation induced injury in mice Commun. Biol. 6 571

Milano F 2013 A python-based software tool for power system analysis 2013 IEEE Power & Energy Society General Meeting (Vancouver, BC, Canada, 21-25 July 2013) (IEEE) pp 1–5

Mumtaz H et al 2020 Age and gender related differences in load-strain response in C57Bl/6 mice Aging 12 24721–33

Oliveira A R D 1987 Un répertoire des accidents radiologiques 1945–1985 Radioprotection 22 89–135

Rottensteiner-Brandl U et al 2017 Influence of different irradiation protocols on vascularization and bone formation parameters in rat femora Tissue Eng.C 23 583–91

Sanner M F 1999 Python: a programming language for software integration and development J. Mol. Graph. Model. 17 57–61

Siddiqui J A and Partridge N C 2016 Physiological bone remodeling: systemic regulation and growth factor involvement Physiology 31 233–45

Somerville J M, Aspden R M, Armour K E, Armour K J and Reid D M 2004 Growth of C57Bl/6 mice and the material and mechanical properties of cortical bone from the tibia Calcified Tissue Int. 74 469–75

Thorne M C 2022 Responding to radiation accidents: what more do we need to know? J. Radiol. Prot. 42 031003

Trompier F et al 2007 EPR dosimetry for actual and suspected overexposures during radiotherapy treatments in Poland Radiat. Meas. 42 1025–8

Trompier F et al 2023 Commentary: minimum reporting standards should be expected for preclinical radiobiology irradiators and dosimetry in the published literature Int. J. Radiat. Biol. 11 1–6

Trompier F, Bassinet C, Wieser A, De Angelis C, Viscomi D and Fattibene P 2009 Radiation-induced signals analysed by EPR spectrometry applied to fortuitous dosimetry Ann. Ist. Super. Sanita 45 287–96

Wong J et al 2008 High-resolution, small animal radiation research platform with x-ray tomographic guidance capabilities Int. J. Radiat.Oncol.*Biol.*Phys. 71 1591–9

Zhai J, He F, Wang J, Chen J, Tong L and Zhu G 2019 Influence of radiation exposure pattern on the bone injury and osteoclastogenesis in a rat model Int. J. Mol. Med. 11 2265–75